Environmental Science & Technology

Article

Cite This: Environ. Sci. Technol. 2019, 53, 5052−5061

pubs.acs.org/est

A Coupled Global Atmosphere-Ocean Model for Air-Sea Exchange of Mercury: Insights into Wet Deposition and Atmospheric Redox Chemistry

Yanxu Zhang,[*,†] Hannah Horowitz,[‡] Jiancheng Wang,[§] Zhouqing Xie,[*,§] Joachim Kuss,[∥] and Anne L. Soerensen[⊥]

[†]Joint International Research Laboratory of Atmospheric and Earth System Sciences, School of Atmospheric Sciences, Nanjing University, Nanjing, Jiangsu 210023, China

[‡]Department of Atmospheric Sciences, University of Washington, Seattle, Washington 98195, United States

[§]Anhui Province Key Laboratory of Polar Environment and Global Change, School of Earth and Space Sciences, University of Science and Technology of China, Hefei, Anhui 230026, China

[∥]Department of Marine Chemistry, Leibniz Institute for Baltic Sea Research, Rostock-Warnemünde 18119, Germany

[⊥]Department of Environmental Science and Analytical Chemistry, Stockholm University, Stockholm 10691, Sweden

Supporting Information

ABSTRACT: Air−sea exchange of mercury (Hg) is the largest flux between Earth system reservoirs. Global models simulate air−sea exchange based either on an atmospheric or ocean model simulation and treat the other media as a boundary condition. Here we develop a new modeling capability (NJUCPL) that couples GEOS-Chem (atmospheric model) and MITgcm (ocean model) at the native hourly model time step. The coupled model is evaluated against high-frequency simultaneous measurements of elemental mercury (Hg^0) in both the atmosphere and surface ocean obtained during five published cruises in the Atlantic, Pacific, and Southern Oceans. Results indicate that the calculated global Hg net evasion flux is 12% higher for the online model than the offline model. We find that the coupled online model captures the spatial pattern of the observations; specifically, it improves the representation of peak seawater Hg^0 (Hg^0_{aq}) concentration associated with enhanced precipitation in the intertropical convergence zone in both the Atlantic and the Pacific Oceans. We investigate the causes of the observed Hg^0_{aq} peaks with two sensitivity simulations and show that the high Hg^0_{aq} concentrations are associated with elevated convective cloud mass flux and bromine concentrations in the tropical upper troposphere. Observations of elevated Hg^0_{aq} concentrations in the western tropical Pacific Ocean merit further study involving BrO vertical distribution and cloud resolving models.

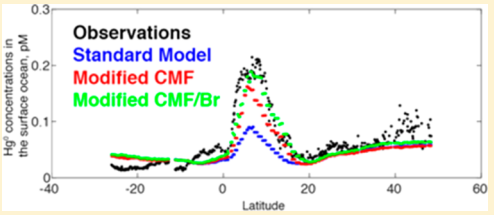

INTRODUCTION

Air−Sea exchange of mercury (Hg) is a bidirectional process that includes the deposition of divalent (Hg^{II}) and elemental (Hg^0) mercury from atmosphere to ocean and the evasion of Hg^0 from the ocean to the atmosphere. It is the largest Hg flux term between environmental media in the Earth system.[1−3] The reduction of deposited Hg^{II} to Hg^0 in the surface ocean followed by air−sea exchange extends the lifetime of Hg in actively cycling reservoirs.[1,4] This process governs the size of the Hg^{II} pool in the surface ocean, which is scavenged by particulate matter to the subsurface ocean and is also the substrate for conversion to the most toxic form of Hg, methylmercury.[5,6] Even though the air−sea exchange process involves both atmospheric and oceanic processes, current global models represent only one of the two compartments and treat the other media as a spatially and/or temporally averaged boundary condition.[7−10] Here we develop a new online coupled model for Hg that couples two state-of-the-art three-dimensional atmosphere and ocean models and use it to examine factors controlling the air−sea exchange fluxes at the atmosphere−ocean interface.

Wet deposition constitutes the main flux of Hg^{II} to the surface ocean and is largely influenced by the amount and type of precipitation.[3,11] Enhanced surface ocean Hg concentrations have been observed in tropical oceans associated with elevated precipitation in the Intertropical Convergence Zone (ITCZ).[12,13] It has also been shown that strong convective systems that reach higher altitudes result in higher Hg concentrations in precipitation than weaker convective and stratiform systems.[14,15] Dry deposition of Hg^{II} in the marine boundary layer is a function of the Hg^{II} concentrations and the deposition velocity, and it is governed by uptake into sea-salt aerosols followed by deposition.[16] Air−Sea exchange of

Received: November 3, 2018
Revised: February 14, 2019
Accepted: April 4, 2019
Published: April 4, 2019

DOI: 10.1021/acs.est.8b06205
Environ. Sci. Technol. 2019, 53, 5052−5061

gaseous Hg^0 is a diffusion process, and the direction of the net exchange is determined by the Hg^0 concentration gradient normalized by the Henry's Law constant across the air−sea interface.[17] The mass transfer coefficient is influenced by factors such as the kinematic viscosity of seawater, aqueous diffusion coefficient of Hg^0, the wave condition, and the turbulence in the air and water surface microlayers.[17,18] The transfer across the surface microlayers is dominated by the water phase and typically parametrized as a function of the wind speed in Hg models.[9,19]

Early box model studies used averaged atmospheric and oceanic Hg concentrations and wind speed to estimate Hg^0 air−sea exchange fluxes.[20−22] In later global three-dimensional atmospheric models spatial variable evasion was estimated based on temperature and sea ice fractions.[8,23] The GEOS-Chem model first traced surface ocean Hg concentrations and air−sea exchange by adding a two-dimensional slab surface ocean module.[17,19] The global three-dimensional ocean Hg models (OFFTRAC, MITgcm, and NEMO) developed later include the isopycnal and diapycnal transport of Hg, but they have prescribed atmospheric Hg deposition fluxes and concentrations.[9,10,24] Previous studies coupling atmosphere and ocean models have used a monthly interval for information exchange, which is appropriate for long-term trend analysis and climatological mean studies.[3,25] However, using monthly intervals smooths out high-frequency signals and hampers our ability to critically evaluate modern high-resolution measurements (every 5 min or higher) in both atmosphere and ocean. This is especially problematic, since air−sea exchange is strongly influenced by episodic high wind speed and precipitation events.[13,26] Indeed, a coupled regional scale atmosphere−ocean model showed better agreement with observed Hg^0 concentrations than previous offline models.[27]

Here we develop a global online model for Hg that couples the GEOS-Chem atmospheric model and the MITgcm ocean model. The models exchange atmospheric Hg^{II} deposition fluxes and ocean Hg^0 net evasion fluxes in a two-way fashion using an hourly time step. We use the coupled model to better understand factors controlling the concentrations and air−sea exchange fluxes of Hg at the atmosphere−ocean interface by comparing model simulations with previously published Hg^0 concentrations from several ocean basins. A specific focus is put on the high surface ocean Hg^0 concentrations observed in the ITCZ regions.

METHODOLOGY

GEOS-Chem Model. We use the GEOS-Chem Hg model (version v9-02) (www.geos-chem.org), which is described (including an evaluation against available observations) by Horowitz et al.[3] for the atmospheric simulation. The model is driven by assimilated meteorological data archived from the Goddard Earth Observing System (GEOS) general circulation model operated by the NASA Global Modeling and Assimilation Office (GMAO). It includes 47 vertical levels extending up to the mesosphere and is run at a horizontal resolution of 4° × 5° by regridding the native GEOS-5 (2007−2012, 1/2° × 2/3°) and GEOS-FP (2013−2017, 1/4° × 5/16°) meteorological data. Two separate tracers, namely, Hg^0 and Hg^{II}, are included. They are transported by the same advection scheme as the GEOS model to achieve consistency. Convective cloud mass fluxes are used to compute convective transport, and a nonlocal scheme is adopted for boundary layer mixing.[28] Hg^{II} is water-soluble and scavenged by precipitation in the forms of both rain and snow. Cold/mixed precipitation is also considered for Hg^{II} absorbed to aerosols.[29,30] A dry deposition velocity is calculated based on the resistance-in-series scheme for both Hg^0 (except over the ocean, where deposition is handled by the air−sea exchange module) and Hg^{II}.[31]

The model uses a global anthropogenic emission inventory for Hg developed by Zhang et al.[32] A recently developed mechanism for Hg^0/Hg^{II} redox chemistry is included,[3] with the concentrations of the principle Hg oxidant, Br, also taken from the GEOS-Chem model.[33] The partitioning of Hg^{II} between the gas phase and particulate matter is assumed to be an instantaneous process and is, except for in the marine boundary layer (MBL), calculated based on a temperature-dependent partitioning coefficient and the mass of fine particulate matter.[30] In the MBL, the partitioning is instead modeled as a first-order process limited by mass transfer of gaseous Hg^{II} onto sea-salt particles, which undergo fast deposition.[2,16] The model also considers the re-emission of Hg^0 from soil based on Smith-Downey et al.[34] with spatial allocation following Selin et al.[7] Emissions from snowpack and re-emission of deposited Hg are modeled following Selin et al.[7] The original two-dimensional slab ocean module is disabled in this study,[17,19] and the air−sea exchange of Hg^0 at the atmosphere−ocean interface is handled by the MITgcm and a newly developed coupler (see section of Model Coupling).

MITgcm Model. The Massachusetts Institute of Technology General Circulation Model (MITgcm) is used in this study to simulate the chemistry and transport of Hg in the ocean. It has a nominal horizontal resolution of 1° × 1° and 50 vertical levels. The resolution is higher over the equator (~0.5° × 1°) and the Arctic (~40 km) to better represent the ocean currents there. The physical ocean is configured as a nonlinear inverse modeling framework with a solution that represents the ocean state for 1992−2011 including seawater temperature, salinity, velocity, sea ice, and turbulent diffusion coefficients (ECCO v4).[35] The model solves the hydrostatic Boussinesq equation[36] and is forced by 6 h ERA-Interim reanalysis fields for the atmosphere (temperature, wind stress, precipitation, humidity, downward radiation) and seasonal climatological runoff.[35]

Hg chemistry and transport were added to this model by Zhang et al.[24] and have been extensively evaluated against observations in the global ocean. The model includes Hg^0, inorganic Hg^{II}, and particulate divalent Hg (Hg^P). It receives atmospheric deposition of Hg^{II} to the surface ocean and includes photochemical and biological redox reactions between Hg^0 and Hg^{II} following Soerensen et al.[19] The partitioning between Hg^{II} and Hg^P is calculated based on a constant partition coefficient and local particulate organic carbon (POC) concentrations. Hg^P is scavenged by POC to the deeper ocean (i.e., the biological pump). The ocean biogeochemistry and ecological variables (e.g., POC) are from the Darwin model.[37] The air−sea exchange flux of Hg^0 is calculated in the MITgcm following Soerensen et al.[19] with a Hg^0 gas exchange velocity from Nightingale et al.,[38] the Henry's law constant from Andersson et al.,[39] Schmidt number for CO_2 from Poissant et al.,[40] and temperature and salinity-corrected Hg^0 diffusivity from Wilke and Chang.[41] The initial conditions of ocean Hg concentrations are from Zhang et al.[25]

Model Coupling. We develop a new coupler (NJUCPL) that facilitates the two-way coupling of GEOS-Chem and MITgcm at their native time resolution (1 h) (the flowchart of the coupling process is shown in Figure S1). The two models

DOI: 10.1021/acs.est.8b06205
Environ. Sci. Technol. 2019, 53, 5052−5061

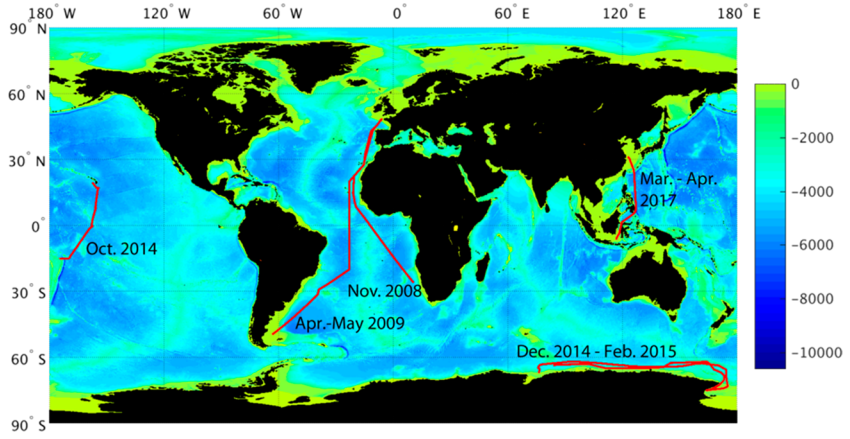

Figure 1. Tracks for the cruises with data adopted in this study. Background color is the bathymetry (m).

Table 1. Summary of Model-Observation Comparisons across Different Cruise Studies in the Global Ocean

	observations[a]			standard model			model with enhanced CMF		model with enhanced CMF/Br	
cruises	n	Hg^0_{atm}[b]	Hg^0_{aq}[c]	n	Hg^0_{atm}	Hg^0_{aq}	Hg^0_{atm}	Hg^0_{aq}	Hg^0_{atm}	Hg^0_{aq}
Central Pacific 2011	548	1.2 ± 0.084	0.066 ± 0.029	548	1.2 ± 0.12	0.075 ± 0.021	1.2 ± 0.14	0.094 ± 0.045	1.2 ± 0.15	0.11 ± 0.055
Atlantic 2009	657	0.81 ± 0.20	0.039 ± 0.020	657	1.2 ± 0.29	0.053 ± 0.015	1.1 ± 0.30	0.054 ± 0.015	1.1 ± 0.30	0.058 ± 0.018
Atlantic 2008	405	0.86 ± 0.23	0.066 ± 0.051	405	1.2 ± 0.20	0.043 ± 0.016	1.1 ± 0.21	0.052 ± 0.032	1.2 ± 0.21	0.061 ± 0.042
Western Pacific 2017	46	1.3 ± 0.20	0.22 ± 0.042	46	1.6 ± 0.58	0.069 ± 0.019	1.7 ± 0.60	0.093 ± 0.034	1.7 ± 0.60	0.11 ± 0.047
Southern Ocean 2014–2015	44	0.94 ± 0.12	0.12 ± 0.067	44	1.0 ± 0.22	0.10 ± 0.020	0.90 ± 0.38	0.15 ± 0.028	0.90 ± 0.38	0.15 ± 0.028

[a]Numbers are arithmetic means and standard deviation. [b]Units: nanograms per cubic meter. [c]Units: picomolar.

are run in parallel and exchange information using intermediate files. The coupler determines when atmospheric Hg^{II} deposition and Hg^0 concentrations are passed from GEOS-Chem to MITgcm and also when the net ocean Hg^0 evasion flux passes from MITgcm to GEOS-Chem (which may be negative if Hg^0 is absorbed at the ocean surface rather than evaded). The resulting files are read by the other model only after the coupler interpolates between the two different horizontal grids. The particular model or the coupler reading the data is paused, until the necessary files have been written. As the size of the files used for the information exchange is small (<100 Kb), the coupler does not significantly slow the slowest of the models (the MITgcm).

Data. We include observational data from five cruises with high-resolution simultaneous measurements of atmospheric and aqueous Hg^0 concentrations in the Atlantic, Pacific, and Southern Oceans (Figure 1 and Table 1). This includes data from Kuss et al.[12] obtained along two north–south transects in the Atlantic Ocean, one in November 2008 (from Bremerhaven, Germany, to Cape Town, South Africa), and the other in April–May 2009 (from Punta Arenas, Chile, to Bremerhaven). We include data reported by Soerensen et al.[13] along a latitudinal transect (~20° N to ~15° S) on the METZYME cruise in the Central Pacific Ocean in October, 2011. Also included are data gained during a cruise along the Antarctic coast.[42] This cruise started from Prydz Bay, Ross Sea, and went to Christchurch, New Zealand, before returning to Prydz Bay during December 2014 to Feburary 2015. The last data set was obtained during the fourth leg of the Chinese National Antarctic Research Expedition (CHINARE) campaign in March–April, 2017 that covered the tropical Indian/Pacific Ocean.[43] Similar measurement methods were used in all these studies, which included a Tekran instrument for atmospheric Hg^0 measurements and an automatic continuous equilibrium system for seawater Hg^0 measurements. The frequency of data reported ranged from 1 to ~10 h. We refer to these data sets by the ocean name and the sample year [e.g., Atlantic (2008), Pacific (2011)].

RESULTS AND DISCUSSION

Exchange Fluxes. Figure 2 compares the annual mean Hg^0 evasion, Hg^{II} deposition, and net atmosphere to ocean transfer (≡ Hg^{II} deposition − Hg^0 net evasion) fluxes simulated by the online model with that of the offline model presented in Horowitz et al.[3] The latter uses archived monthly mean surface ocean Hg concentrations from the MITgcm to drive the GEOS-Chem model (we refer to it as the "offline model"). Overall, the spatial patterns of the fluxes are similar, indicating that the offline model is able to capture long-term means and large-scale variability. The global total net Hg evasion flux calculated by the online model is 3360 Mg/a, which is 12% higher than the offline model (3000 Mg/a). Since the Hg processes in the surface ocean and the marine boundary layer are so closely linked an increase in the Hg^0 evasion flux correspondingly increases the Hg^{II} deposition over the ocean (Figure 2C,D). However, such changes are mainly limited to marine boundary layer processes, and the impact on the atmospheric and terrestrial Hg burden is not significant. Besides the difference in modeling setup for atmosphere-ocean coupling, the increase in the evasion flux is also associated with model resolution: the online model is simulating the air–sea exchange processes at a nominal resolution of 1° × 1° (MITgcm), while the offline model uses 4° × 5° (GEOS-

DOI: 10.1021/acs.est.8b06205
Environ. Sci. Technol. 2019, 53, 5052–5061

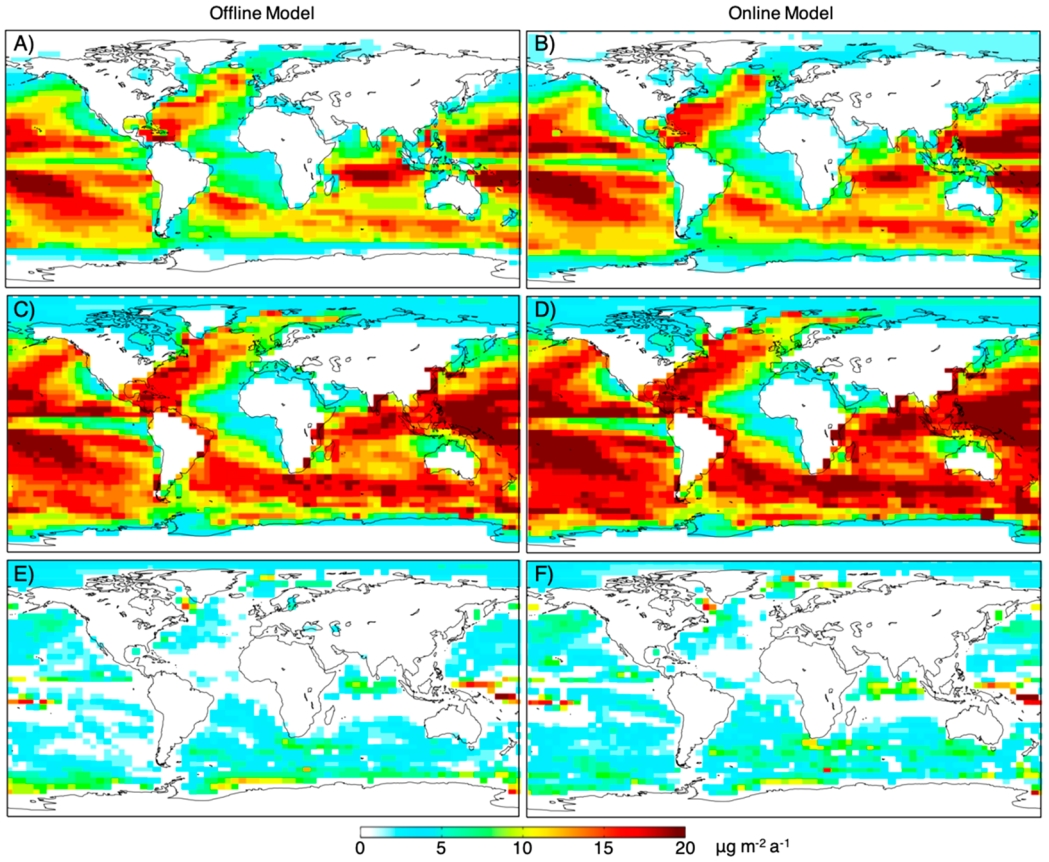

Figure 2. Comparison of annual total Hg^0 net evasion (A, B), Hg^{II} deposition (C, D), and net atmosphere to ocean transfer flux (≡ Hg^{II} deposition − Hg^0 net evasion, E, F) between offline (A, C, E) and online (B, D, F) models.

Chem). When regridding high-resolution wind fields to a lower resolution, winds, which have opposite directions in the finer grid, are canceled out in the coarser model grid. This decreases the mean of the square of the wind speed (Figure S2). As the exchange velocity of Hg^0 (piston velocity) is a function of the square of the wind speed, this decrease will subsequently lower the calculated Hg^0 exchange fluxes. This, in part, explains the differences in calculated evasion fluxes for the two resolutions. From this we hypothesize that the modeled evasion flux will continue to increase as model resolution increases. We suggest that a resolution of ∼0.2° × 0.2° will be optimal for the piston velocity scheme we use, as it is based on averaged SF_6 concentrations and wind speeds at approximately this scale.[38]

Model Evaluation. Figure 3 and Table 1 show the model-observation comparison for Hg^0 concentrations in the marine boundary layer (Hg^0_{atm}) and the surface ocean (Hg^0_{aq}) along the cruise tracks shown in Figure 1 (blue lines for the Standard Model). In the two Atlantic (2008, 2009) and the Central Pacific cruises (2011) Hg^0_{aq} concentration peaks were observed in the Tropics. Peak concentrations are 0.1−0.2 pM, which are 2−3 times higher than the corresponding cruise-average concentrations (Table 1). These enhancements have been attributed to elevated Hg inputs through wet deposition in the ITCZ.[12,13] This is supported by observations of total Hg concentrations in precipitation over tropical regions of 10−55 and 14−75 pM in the Atlantic and the Pacific Oceans, respectively,[44−46] which are much higher than that in seawater (∼1 pM). Hg^{II} deposited in precipitation can be rapidly reduced to Hg^0 through photochemical reduction in the surface ocean.[47] For the western Pacific 2017 cruise, a similar but less obvious peak Hg^0_{aq} concentration is observed at 2° S. The average observed Hg^0_{aq} concentration (0.22 ± 0.042) during this cruise is approximately a factor of 2 higher than the other three tropical cruises.

Observed Hg^0_{atm} concentrations from the Pacific (2011) and Atlantic (2008, 2009) cruises show a different spatial variability than Hg^0_{aq}. This is because Hg^0_{atm} has a lifetime of several months that enables it to be relatively well-mixed at hemispheric scales. The observed Hg^0_{atm} has an ∼0.2−0.4 ng/m^3 concentration gradient across the two hemispheres, reflecting the difference in anthropogenic Hg emissions.[2] For the Pacific 2017 cruise the Hg^0_{atm} concentration only changes significantly north of ∼28° N, where it is influenced by the outflow plume of East Asian emissions.[48] Over the Southern Ocean, observations show little zonal variability in either Hg^0_{aq} (0.12 ± 0.067) or Hg^0_{atm} (0.94 ± 0.12) concentrations.

The model generally captures the spatial patterns of Hg^0_{aq} and Hg^0_{atm} concentrations observed during the Atlantic (2008, 2009), Pacific (2011), and Southern Ocean (2015) cruise studies, and the modeled Hg^0_{aq} concentrations are not significantly different from observations (Table 1). For the Pacific (2011) cruise, for example, the model results (Hg^0_{aq}: 0.075 ± 0.021 pM, Hg^0_{atm}: 1.2 ± 0.12 pM) are not significantly different from the observations (Hg^0_{aq}: 0.066 ± 0.029 pM, Hg^0_{atm}: 1.2 ± 0.084 pM) (t test on means, α = 0.05). The modeled Hg^0_{atm} concentrations are significantly higher than observations over the two Atlantic cruises, but they have similar interhemisphere gradients (Table 1 and Figure 3).

Gas Exchange Parameterizations. There are different parametrizations to calculate the gas exchange velocity of

DOI: 10.1021/acs.est.8b06205
Environ. Sci. Technol. 2019, 53, 5052−5061

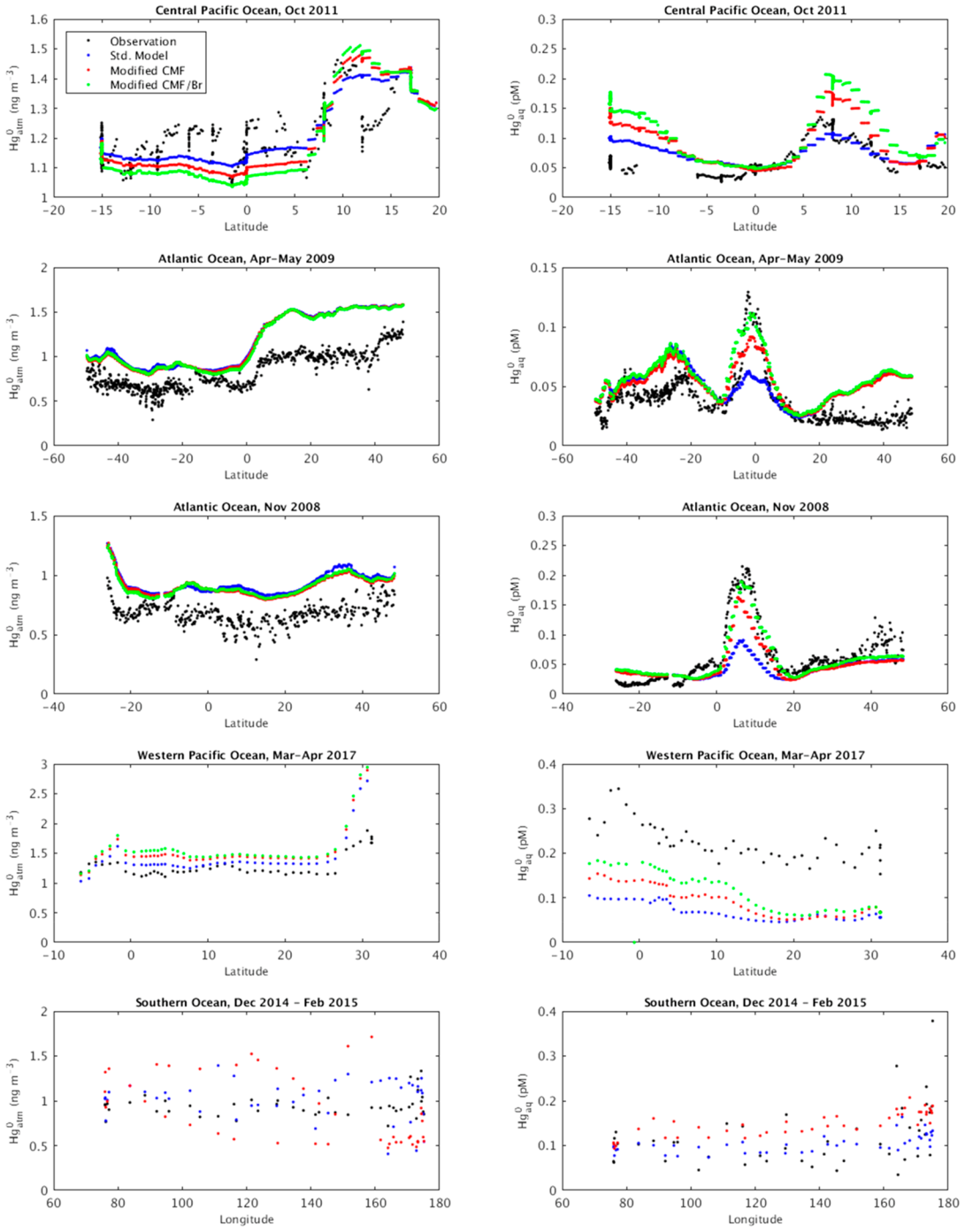

Figure 3. Comparison of observed (black dots) and modeled (blue: standard model, red: with enhanced cloud mass flux in the tropical high troposphere, green: with enhanced cloud mass flux and Br/BrO concentrations in the tropical high troposphere) Hg^0 concentrations in the marine boundary layer (left) and the surface ocean (right) in cruise studies shown in Figure 1.

Hg^0.[38,49−52] Each parametrization relates the exchange velocity to wind speed based on different data sets (Table S1). Figure 4 shows the difference between annual mean Hg^0 evasion fluxes for each of the parametrizations and that calculated by Nightingale et al.[38] (i.e., the Standard Model, Figure 2B). The latter is preferred and widely adopted, because it was developed from in situ experiments with both volatile and nonvolatile tracers.[53] We find that these methods predict similar global total Hg^0 evasion fluxes in spite of larger regional differences. Indeed, the calculated global total annual Hg^0 fluxes range from 2840 to 3710 Mg a^{-1}, which are −16% to +10% different from the Standard Model. The Liss and Merlivat 1986[49] method predicts lower fluxes almost everywhere (Figure 4A), while the Wanninkhof 1992[50] method results in higher fluxes especially over the tropical regions (Figure 4B). The Wanninkhof and McGillis 1999[51] method, which adopts a third-order term for wind speed, results in a global total flux similar to the Standard Model but has higher evasion fluxes over high-wind-speed regions in the high latitudes (+20−30%) and lower fluxes over calm low latitudes (−10−25%, Figure 4C). The McGillis 2001[52] method is

DOI: 10.1021/acs.est.8b06205
Environ. Sci. Technol. 2019, 53, 5052−5061

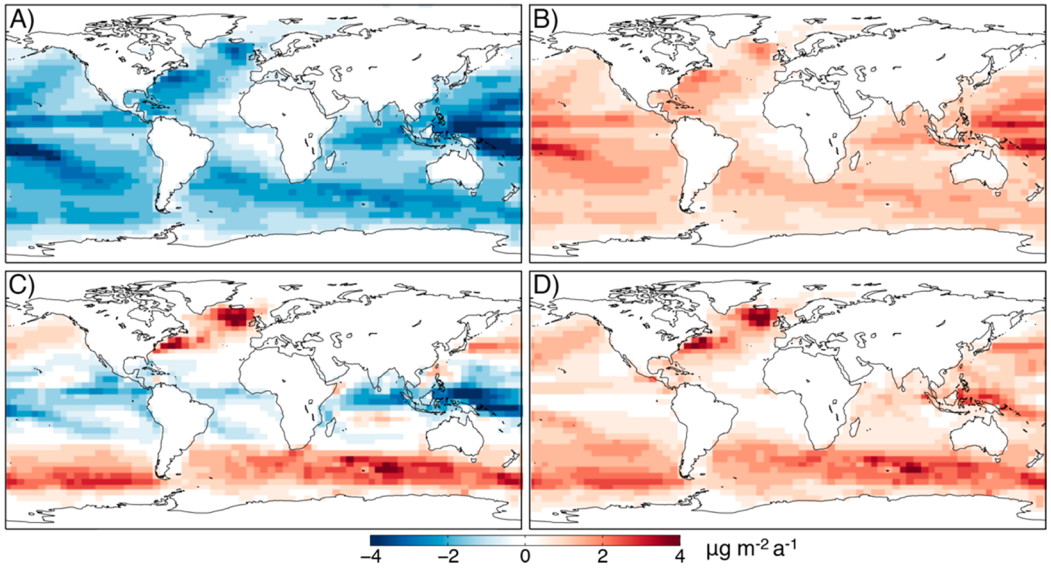

Figure 4. Difference of annual mean net Hg^0 evasion flux calculated by different gas exchange parametrizations over the global ocean. Panels show the difference with that calculated by Standard Model (Ninghtingale et al.,[33] Figure 3B). (A) Liss and Merlivat;[49] (B) Wanninkhof;[50] (C) Wanninkhof and McGillis;[51] (D) McGillis et al.[52] The details of gas exchange parametrizations are available in Table S1.

Table 2. Summary of Model-Observation Comparisons for Hg^0_{aq} Peak Magnitudes and Locations across Different Cruise Studies in the Tropical Ocean

	observations		standard model		model with enhanced CMF		model with enhanced CMF/Br	
cruises	magnitude	latitude	magnitude	latitude	magnitude	latitude	magnitude	latitude
Central Pacific 2011	0.14	7° N	0.11	8° N	0.18	7° N	0.21	7° N
Atlantic 2009	0.13	2° S	0.085	2° S	0.091	1° S	0.11	1° S
Atlantic 2008	0.22	7° N	0.090	7° N	0.16	6° N	0.19	6° N
Western Pacific 2017	0.34	3° S	0.11	5° S	0.15	5° S	0.18	5° S

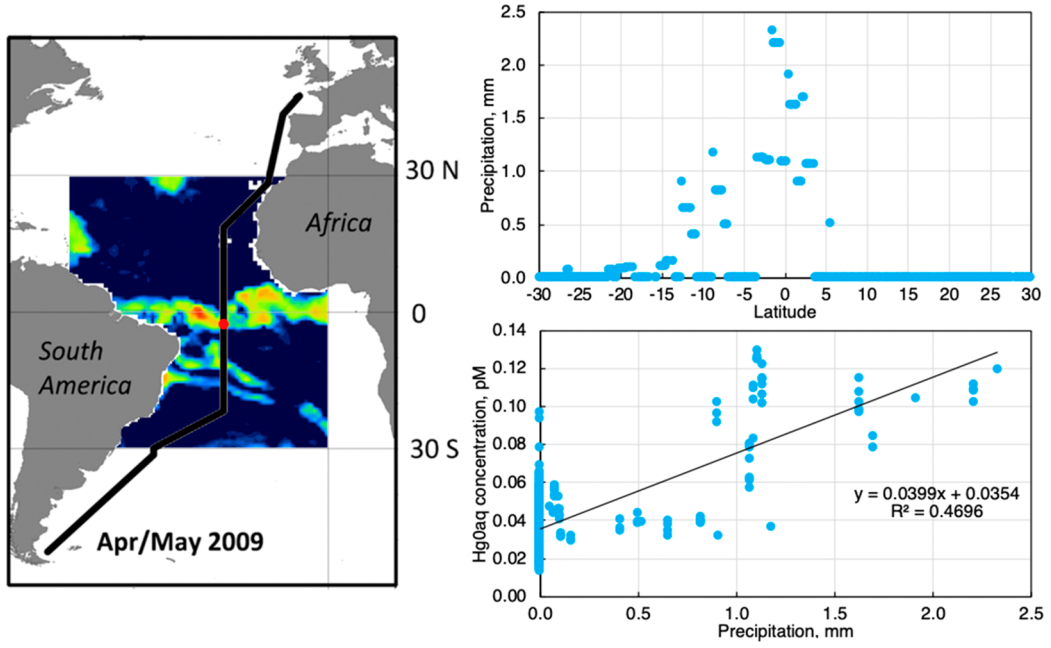

Figure 5. Case analysis of peak Hg^0_{aq} concentration observed on May 4, 2009, by Kuss et al. (2011). (A) Cruise track on top of precipitation depth (at 18:00 UTC; red and orange colors indicate heavy precipitation, and blue means no rain) from GEOS-5 meteorological data. The red spot on the cruise track indicates the research vessel location. (B) 6 h precipitation depth along the cruise track when the research vessel is present. (C) Relationship between the precipitation data in (B) and observed Hg^0_{aq} concentrations at the same location.

similar to the Wanninkhof and McGillis 1999 method (Figure 4D).

We use the Atlantic (2009) cruise as a case study to evaluate the impact of different gas exchange parametrizations on

DOI: 10.1021/acs.est.8b06205
Environ. Sci. Technol. 2019, 53, 5052−5061

modeled Hg^0_{aq} and Hg^0_{air} concentrations (Figure S3). We find that the different parametrizations result in similar spatial patterns. The difference among gas exchange parametrizations ranges from −13% to +9.5% for Hg^0_{air} and from −11% to +36% for Hg^0_{aq}, which are within the uncertainty range of Hg^0 observations and the model-observation differences. It indicates that it is not possible to use the current model framework in combination with available Hg^0 observations to determine which parametrization is more accurately calculating the gas exchange velocities. Direct measurements of Hg^0 fluxes combined with simultaneous measurements of parameters other than wind speed (e.g., temperature, salinity, wave, bubble, and biological film conditions) are required.

Precipitation. The model captures the latitude of the observed tropical Hg^0_{aq} peaks well (Table 2). The peaks are observed at ∼7° N, ∼2° S, and ∼7° N in the Pacific (2011), Atlantic (2009), and Atlantic (2008) cruises, respectively, while the model locates them at ∼8° N, ∼2° S, and ∼7° N. This is a significant improvement compared with the offline model used by Soerensen et al.,[13] which simulated a peak for Hg^0_{aq} in the Atlantic (2009) cruise at ∼9° N (∼2° S in the observation). This improvement is achieved by a better representation of the precipitation in the online model (Figure 5). Indeed, the peak Hg^0_{aq} concentration is observed exactly when the precipitation along the cruise track is at its maximum. Figure 5A shows that the research vessel was crossing a heavy rainfall belt at the time peak Hg^0_{aq} concentrations were observed. There is furthermore a linear relationship between Hg^0_{aq} concentrations and precipitation for this cruise:

$$[Hg^0_{aq}] = 0.040 \times P + 0.035, \quad r^2 = 0.47 \tag{1}$$

where $[Hg^0_{aq}]$ is the observed Hg^0_{aq} concentrations in picomolar, and P is the 6 h precipitation from the GEOS-5 reanalysis product (mm) at the same location and time as the observations are conducted. The offline model, using monthly averaged deposition, cannot follow the position of the rain belt during the seasonal north−south shift of the ITCZ.

While the model has no significant low bias over midlatitudes and polar regions (Figure 3) and improves the ability to capture the location of the Hg^0_{aq} concentration peaks, it still significantly underestimates the magnitude of the peaks except for the Pacific (2011) cruise. In the Atlantic (2008) and (2009) cruises the observed peaks are 0.22 and 0.13 pM, respectively, while the modeled values are only 0.090 pM (−60% low bias) and 0.085 pM (−35% low bias). The largest underestimate occurs for the Pacific (2017) cruise (0.11 pM vs 0.34 pM, ca. −70% low bias). The underestimation of the peak Hg^0_{aq} concentrations is likely caused by insufficient Hg deposition in the ITCZ as suggested by Soerensen et al.[13] However, such a hypothesis could not be quantitatively tested by the offline model framework used by Soerensen et al., and the observed high peak concentrations could not be fully explained. We therefore use our online coupled model to test their hypothesis on driving factors of the surface ocean Hg^0_{aq} concentrations in this region with two sensitivity simulations presented below.

Convective Cloud Mass Flux. Even though the GEOS-5 total precipitation data reproduce the satellite observations over the tropical oceans (Tropical Rainfall Measuring Mission, https://pmm.nasa.gov/data-access/downloads/TRMM) (Figure S4), the coarse resolution of the GEOS-Chem model (4° × 5°) cannot resolve individual convective cells and thus underestimates the frequency of precipitation events originating in the upper troposphere.[13] This may cause a significant low bias in the Hg deposition, as Hg^{II} concentrations are ∼2 orders of magnitude higher in the upper troposphere than at the surface due to lower temperatures and higher Br concentrations that favor its formation.[2,54] In a previous study, Zhang et al.[14] found that a higher horizontal resolution (0.5° × 0.666°) helped resolve the model underestimation of Hg wet deposition over the southeast United States. Indeed, we find that large subgrid variability in cloud top temperature (which is inversely related to cloud height) is observed by satellite in tropical regions (GridSat-B1 product from NCEI, 0.07° resolution, http://www.ncdc.noaa.gov/gridsat). For example, during the observed Hg^0_{aq} peak of the Atlantic (2009) cruise (23° W 2.4° S, May 4, 2009 18:00 coordinated universal time (UTC), as shown in Figure 5A), the cloud top temperature was 253 K, which is derived from the GEOS archived outgoing longwave radiation and is calculated based on the Stefan−Boltzmann law. On the one hand, this means the cloud top height is at ∼8 km height based on the archived GEOS-5 temperature profile. On the other hand, there are ∼4000 Gridsat-B1 grid cells in this 4° × 5° gridbox of GEOS-5 data. Even though the mean value of these boxes is close to GEOS-5 (260 K), approximately one-third of the cells are lower than 240 K with a minimum of 196 K (Figure S5). This indicates the existence of cloud mass up to an altitude of ∼14 km. The fact that GEOS-Chem is not able to correctly predict the cloud mass and subsequent precipitation and wet deposition between the 8−14 km height range is a likely cause of the underestimation of Hg^0_{aq} concentrations in the ITCZ regions by our simulation.

In a sensitivity run, we adjust the cloud mass flux (CMF) of the GEOS-5 and GEOS-FP meteorological data, which is used by the GEOS-Chem model to calculate convection and the associated wet deposition. As no observed field of CMF is available, we use the difference between two data versions (GEOS-4 and GEOS-5) to test how sensitive the Hg model simulation is to this meteorological factor and refer to this sensitivity run as "Modified CMF" (compared with the "Standard Model"). The GEOS-4 data has higher CMF over the tropical regions than the GEOS-5 (Steven Pawson, GMAO activities and partnership with GEOS-Chem, The fourth GEOS-Chem Scientific and Users' Meeting, Harvard University, April 7−10, 2009). We scale up the flux over the tropics based on the ratio of GEOS-4 and GEOS-5 data, which varies both horizontally and vertically. This results in scaling factors ranging from 2 to 12 at a latitude band of 15° S−15° N and altitudes higher than 600 hPa. Figure 3 and Table 1 show the results of the Modified CMF simulation. We find that the adjustment to the CMF increases the peak Hg^0_{aq} concentrations for the four tropical cruises to 0.091, 0.16, 0.18, and 0.15 pM for Atlantic (2009), (2008), Pacific (2011), and (2017), respectively. This is 44 to 129% of the observed values, and the average bias is reduced from −46% in the Standard Model to −21%. This shows that the Hg^0_{aq} concentrations along the ITCZ are sensitive to the deep convection strength above 600 hpa and strengthen the hypothesis that the active deep convection makes a significant contribution to the elevated seawater Hg concentrations in this region.

Atmospheric Hg Redox Chemistry. Another cause of the high Hg_{0aq} concentrations in the ITCZ regions could be the high atmospheric Hg^{II} concentrations in the tropical upper troposphere. Limited observations in North America and

DOI: 10.1021/acs.est.8b06205
Environ. Sci. Technol. 2019, 53, 5052−5061

Europe show increasing atmospheric Hg^{II} concentrations with altitude in the troposphere until the tropopause.[54] The GEOS-Chem model, using Br as the main oxidant, generally captures this trend but not the absolute magnitudes.[13] Horowitz et al.[3] updated the reaction mechanism of Holmes et al.[2] and incorporated new reaction rate constants for $Br+Hg^0$ and second-stage oxidation by NO_2 and HO_2 radicals. The latter helps to increase Hg^{II} concentration and wet deposition over low-latitude regions;[3] however, we suggest that it may still be biased low.

One reason for this low Hg^{II} bias is an underestimation of the Br concentration in our atmospheric model. Indeed, Schmidt et al.[33] found the modeled BrO concentrations (which is directly retrievable by optical instruments and is in fast equilibrium with Br) were biased low in the tropical upper troposphere when compared with observed vertical profiles over the Pacific Ocean. This underestimation of Br leads to an underestimation of Hg^{II} in our model simulation.[33,55] We conducted a sensitivity run, in which we increase the Br concentrations to compensate for the low model bias in this region. The Br concentration is doubled over the 7−13 km altitude range (100−400 hPa) in the tropics (22° S−22° N) according to the magnitude of model bias found by Schmidt et al.[33] (refer to Figure 5 and Figure S7). The cloud mass flux is furthermore adjusted as described above for the Modified CMF run. We refer to the result as "Modified CMF/Br", and the result is summarized in Figure 3 and Table 1. We find that adjusting the Br concentrations further increases the peak Hg^0_{aq} concentrations of the four tropical cruises to 0.19, 0.11, 0.21, and 0.18 pM for the Atlantic (2008 and 2009) and Pacific (2011 and 2017) cruises, respectively. This results in a mean bias of −6.5%, which is even closer to observations than the results from the Modified CMF simulation (Figure 3 and Table 2). Thus, with the two sensitivity simulations we show that the model's underestimation of the Hg^0_{aq} peak in the ITCZ may be improved with more accurate representation of convective cloud mass flux and assuming higher Br concentrations at high altitude. We conclude that the high Hg^0_{aq} concentrations in this region are indeed caused by the enrichment of atmospheric Hg^{II} in the upper troposphere that is scavenged down by deep convection and heavy precipitation.

Western Tropical Pacific Ocean. While the Modified CMF/Br reproduces the observed Hg^0_{aq} concentrations in the four tropical cruises well, there is still a relatively large discrepancy between observations and model simulation in the western tropical Pacific Ocean (Pacific 2017 cruise; modeled peak is ca. −50% lower than observed; Figure 3 and Table 2). We suggest two explanations for this. It could be a result of large regional variability in subgrid scale convective activity and that the simple unified scaling factor adopted in the Modified CMF simulation is too low for this region. Further studies that use models with cloud resolving resolution, such as the Weather Research and Forecasting (WRF) model, are therefore needed to better represent the convective mass flux in this region. In addition, observed atmospheric BrO profiles over this part of the ocean are also an urgent need that will allow the Br concentration fields hypothesized in the Modified CMF/Br simulation to be evaluated. The other possible driver of the low bias in this region, which we deem less likely, is associated with the assumptions on main Hg^0 oxidants in the atmosphere. Holmes et al.[2] found that if OH radicals and O_3 are the main oxidants for Hg^0 this results in higher Hg^{II} concentration in the tropical upper troposphere and subsequently higher deposition fluxes in the tropical regions than the Hg+Br mechanism. Indeed, the OH/O_3 mechanism predicts the highest deposition over the western tropical Pacific and Atlantic Oceans (refer to Figure 13 of ref 2). Although it is argued that gas-phase oxidation of Hg^0 by OH and O_3 is too slow to be of atmospheric relevance on the global scale,[2] a two-step mechanism for OH oxidation is possible under atmospheric conditions.[56] The high Hg^0_{aq} concentrations in the western tropical Pacific Ocean regions could support an importance of OH for the atmospheric Hg chemistry, at least in this region.

■ ASSOCIATED CONTENT

Supporting Information

The Supporting Information is available free of charge on the ACS Publications website at DOI: 10.1021/acs.est.8b06205.

A flowchart of the two-way coupling framework, a comparison of wind speed at different resolution, the impact of different gas exchange velocity schemes, an evaluation of model precipitation and cloud top height data, and a table containing details about air−sea exchange velocity methods are provided (PDF)

■ AUTHOR INFORMATION

Corresponding Authors

*E-mail: zhangyx@nju.edu.cn. (Y.-x.Z.)
*E-mail: zqxie@ustc.edu.cn. (Z.-q.X.)

ORCID

Yanxu Zhang: 0000-0001-7770-3466
Jiancheng Wang: 0000-0002-1274-3456
Joachim Kuss: 0000-0001-8586-6265
Anne L. Soerensen: 0000-0002-8490-8600

Notes

The authors declare no competing financial interest.

■ ACKNOWLEDGMENTS

The authors gratefully acknowledge financial support from National Natural Science Foundation of China (NNSFC) 41875148, Start-up fund of the Thousand Youth Talents Plan, Jiangsu Innovative and Entrepreneurial Talents Plan, the Collaborative Innovation Center of Climate Change, Jiangsu Province, and the Swedish Research Council Formas. We thank J.-p. Tang from Nanjing Univ. for helping in high-performance computation, J. Liang, J. Yuan, M.-h. Wang, and H.-l. Yuan from Nanjing Univ. for helpful discussion and interpreting satellite data. The original model codes for the two sensitivity simulations are available upon request.

■ REFERENCES

(1) Amos, H. M.; Jacob, D. J.; Streets, D. G.; Sunderland, E. M. Legacy impacts of all-time anthropogenic emissions on the global mercury cycle. *Glob. Biogeochem. Cycle* **2013**, *27* (2), 410−421.

(2) Holmes, C. D.; Jacob, D. J.; Corbitt, E. S.; Mao, J.; Yang, X.; Talbot, R.; Slemr, F. Global atmospheric model for mercury including oxidation by bromine atoms. *Atmos. Chem. Phys.* **2010**, *10* (24), 12037−12057.

(3) Horowitz, H. M.; Jacob, D. J.; Zhang, Y.; Dibble, T. S.; Slemr, F.; Amos, H. M.; Schmidt, J. A.; Corbitt, E. S.; Marais, E. A.; Sunderland, E. M. A new mechanism for atmospheric mercury redox chemistry: implications for the global mercury budget. *Atmos. Chem. Phys.* **2017**, *17* (10), 6353−6371.

DOI: 10.1021/acs.est.8b06205
Environ. Sci. Technol. 2019, 53, 5052−5061

(4) Corbitt, E. S.; Jacob, D. J.; Holmes, C. D.; Streets, D. G.; Sunderland, E. M. Global source-receptor relationships for mercury deposition under present-day and 2050 emissions scenarios. *Environ. Sci. Technol.* **2011**, *45* (24), 10477−84.
(5) Mason, R.; Fitzgerald, W. F. The distribution and biogeochemical cycling of mercury in the equatorial Pacific Ocean. *Deep Sea Res., Part I* **1993**, *40* (9), 1897−1924.
(6) Fitzgerald, W. F.; Lamborg, C.; Hammerschmidt, C. Marine biogeochemical cycling of mercury. *Chem. Rev.* **2007**, *107*, 641−662.
(7) Selin, N. E.; Jacob, D. J.; Yantosca, R. M.; Strode, S.; Jaegle, L.; Sunderland, E. M. Global 3-D land-ocean-atmosphere model for mercury: Present-day versus preindustrial cycles and anthropogenic enrichment factors for deposition. *Global Biogeochem. Cycles* **2008**, *22* (2), 1−13, DOI: 10.1029/2007GB003040.
(8) Durnford, D.; Dastoor, A.; Ryzhkov, A.; Poissant, L.; Pilote, M.; Figueras-Nieto, D. How relevant is the deposition of mercury onto snowpacks? − Part 2: A modeling study. *Atmos. Chem. Phys.* **2012**, *12* (19), 9251−9274.
(9) Zhang, Y.; Jaeglé, L.; Thompson, L. Natural biogeochemical cycle of mercury in a global three-dimensional ocean tracer model. *Glob. Biogeochem. Cycle* **2014**, *28* (5), 553−570.
(10) Semeniuk, K.; Dastoor, A. Development of a global ocean mercury model with a methylation cycle: outstanding issues. *Glob. Biogeochem. Cycle* **2017**, *31* (2), 400−433.
(11) Zhang, Y.; Jaeglé, L. Decreases in mercury wet deposition over the united states during 2004−2010: roles of domestic and global background emission reductions. *Atmosphere* **2013**, *4* (2), 113−131.
(12) Kuss, J.; Zülicke, C.; Pohl, C.; Schneider, B. Atlantic mercury emission determined from continuous analysis of the elemental mercury sea-air concentration difference within transects between 50°N and 50°S. *Global Biogeochem. Cycles* **2011**, *25* (3), 1 DOI: 10.1029/2010GB003998.
(13) Soerensen, A. L.; Mason, R. P.; Balcom, P. H.; Jacob, D. J.; Zhang, Y.; Kuss, J.; Sunderland, E. M. Elemental mercury concentrations and fluxes in the tropical atmosphere and ocean. *Environ. Sci. Technol.* **2014**, *48* (19), 11312−9.
(14) Zhang, Y.; Jaeglé, L.; van Donkelaar, A.; Martin, R. V.; Holmes, C. D.; Amos, H. M.; Wang, Q.; Talbot, R.; Artz, R.; Brooks, S.; Luke, W.; Holsen, T. M.; Felton, D.; Miller, E. K.; Perry, K. D.; Schmeltz, D.; Steffen, A.; Tordon, R.; Weiss-Penzias, P.; Zsolway, R. Nested-grid simulation of mercury over North America. *Atmos. Chem. Phys. Discuss.* **2012**, *12*, 2603−2646.
(15) Holmes, C. D.; Krishnamurthy, N. P.; Caffrey, J. M.; Landing, W. M.; Edgerton, E. S.; Knapp, K. R.; Nair, U. S. Thunderstorms increase mercury wet deposition. *Environ. Sci. Technol.* **2016**, *50* (17), 9343−50.
(16) Holmes, C. D.; Jacob, D. J.; Mason, R. P.; Jaffe, D. A. Sources and deposition of reactive gaseous mercury in the marine atmosphere. *Atmos. Environ.* **2009**, *43* (14), 2278−2285.
(17) Strode, S. A.; Jaeglé, L.; Selin, N. E.; Jacob, D. J.; Park, R. J.; Yantosca, R. M.; Mason, R. P.; Slemr, F., Air-sea exchange in the global mercury cycle. *Glob. Biogeochem. Cycle* 2007, *21*, (1), doi: DOI: 10.1029/2006GB002766.
(18) Kuss, J. Water-air gas exchange of elemental mercury: An experimentally determined mercury diffusion coefficient for Hg^0 water-air flux calculations. *Limnol. Oceanogr.* **2014**, *59* (5), 1461−1467.
(19) Soerensen, A. L.; Sunderland, E. M.; Holmes, C. D.; Jacob, D. J.; Yantosca, R. M.; Skov, H.; Christensen, J. H.; Strode, S. A.; Mason, R. P. An improved global model for air-sea exchange of mercury: high concentrations over the North Atlantic. *Environ. Sci. Technol.* **2010**, *44* (22), 8574−8580.
(20) Mason, R. P.; Fitzgerald, W. F.; Morel, F. M. M. The biogeochemical cycling of elemental mercury anthropogenic influences. *Geochim. Cosmochim. Acta* **1994**, *58* (15), 3191−3198.
(21) Lamborg, C.; Fitzgerald, W. F.; O'Donnell, J.; Torgersen, T. A non−steady-state compartmental model of global-scale mercury biogeochemistry with interhemispheric atmospheric gradients. *Geochim. Cosmochim. Acta* **2002**, *66*, 1105−1118.
(22) Sunderland, E. M.; Mason, R. P. Human impacts on open ocean mercury concentrations. *Global Biogeochem. Cycles* **2007**, *21* (4), 1 DOI: 10.1029/2006GB002876.
(23) Ryaboshapko, A.; Bullock, O. R., Jr.; Christensen, J.; Cohen, M.; Dastoor, A.; Ilyin, I.; Petersen, G.; Syrakov, D.; Artz, R. S.; Davignon, D.; Draxler, R. R.; Munthe, J. Intercomparison study of atmospheric mercury models: 1. Comparison of models with short-term measurements. *Sci. Total Environ.* **2007**, *376* (1−3), 228−40.
(24) Zhang, Y.; Jacob, D. J.; Dutkiewicz, S.; Amos, H. M.; Long, M. S.; Sunderland, E. M. Biogeochemical drivers of the fate of riverine mercury discharged to the global and Arctic oceans. *Glob. Biogeochem. Cycle* **2015**, *29* (6), 854−864.
(25) Zhang, Y.; Jaeglé, L.; Thompson, L.; Streets, D. G. Six centuries of changing oceanic mercury. *Glob. Biogeochem. Cycle* **2014**, *28* (11), 1251−1261.
(26) Sigler, J. M.; Mao, H.; Talbot, R. Gaseous elemental and reactive mercury in Southern New Hampshire. *Atmos. Chem. Phys.* **2009**, *9* (6), 1929−1942.
(27) Tomažič, Š.; Ličer, M.; Žagar, D. Numerical modelling of mercury evasion in a two-layered Adriatic Sea using a coupled atmosphere-ocean model. *Mar. Pollut. Bull.* **2018**, *135*, 1164−1173.
(28) Lin, J. T.; McElroy, M. B. Impacts of boundary layer mixing on pollutant vertical profiles in the lower troposphere: Implications to satellite remote sensing. *Atmos. Environ.* **2010**, *44* (14), 1726−1739.
(29) Liu, H.; Jacob, D.; Bey, I.; Yantosca, R. M. Constraints from ^{210}Pb and ^{7}Be on wet deposition and transport in a global three-dimensional chemical tracer model driven by assimilated meteorological fields. *J. Geophys. Res.* **2001**, *106* (D11), 12109−12128.
(30) Amos, H. M.; Jacob, D. J.; Holmes, C. D.; Fisher, J. A.; Wang, Q.; Yantosca, R. M.; Corbitt, E. S.; Galarneau, E.; Rutter, A. P.; Gustin, M. S.; Steffen, A.; Schauer, J. J.; Graydon, J. A.; Louis, V. L. S.; Talbot, R. W.; Edgerton, E. S.; Zhang, Y.; Sunderland, E. M. Gas-particle partitioning of atmospheric Hg(II) and its effect on global mercury deposition. *Atmos. Chem. Phys.* **2012**, *12* (1), 591−603.
(31) Wesely, M. L. Parameterization of surface resistances to gaseous dry deposition in regional-scale numerical-models. *Atmos. Environ.* **1989**, *23* (6), 1293−1304.
(32) Zhang, Y.; Jacob, D. J.; Horowitz, H. M.; Chen, L.; Amos, H. M.; Krabbenhoft, D. P.; Slemr, F.; St Louis, V. L.; Sunderland, E. M. Observed decrease in atmospheric mercury explained by global decline in anthropogenic emissions. *Proc. Natl. Acad. Sci. U. S. A.* **2016**, *113* (3), 526−531.
(33) Schmidt, J. A.; Jacob, D. J.; Horowitz, H. M.; Hu, L.; Sherwen, T.; Evans, M. J.; Liang, Q.; Suleiman, R. M.; Oram, D. E.; Le Breton, M.; Percival, C. J.; Wang, S.; Dix, B.; Volkamer, R. Modeling the observed tropospheric BrO background: Importance of multiphase chemistry and implications for ozone, OH, and mercury. *J. Geophys. Res. Atmospheres* **2016**, *121* (19), 11819−11835.
(34) Smith-Downey, N. V.; Sunderland, E. M.; Jacob, D. J. Anthropogenic impacts on global storage and emissions of mercury from terrestrial soils: Insights from a new global model. *J. Geophys. Res.* **2010**, *115* (G3), 1 DOI: 10.1029/2009JG001124.
(35) Forget, G.; Campin, J. M.; Heimbach, P.; Hill, C. N.; Ponte, R. M.; Wunsch, C. ECCO version 4: an integrated framework for non-linear inverse modeling and global ocean state estimation. *Geosci. Model Dev.* **2015**, *8* (10), 3071−3104.
(36) Marshall, J.; Adcroft, A.; Hill, C.; Perelman, L.; Heisey, C. A finite-volume, incompressible Navier Stokes model for studies of the ocean on parallel computers. *J. Geophys. Res. Oceans* **1997**, *102* (C3), 5753−5766.
(37) Dutkiewicz, S.; Ward, B. A.; Monteiro, F.; Follows, M. J. Interconnection of nitrogen fixers and iron in the Pacific Ocean: Theory and numerical simulations. *Global Biogeochem. Cycles* **2012**, *26* (1), 1 DOI: 10.1029/2011GB004039.
(38) Nightingale, P. D.; Malin, G.; Law, C. S.; Watson, A. J.; Liss, P. S.; Liddicoat, M. I.; Boutin, J.; Upstill-Goddard, R. C. In situ evaluation of air-sea gas exchange parameterizations using novel conservative and volatile tracers. *Glob. Biogeochem. Cycle* **2000**, *14* (1), 373−387.

DOI: 10.1021/acs.est.8b06205
Environ. Sci. Technol. 2019, 53, 5052−5061

(39) Andersson, M. E.; Sommar, J.; Gårdfeldt, K.; Lindqvist, O. Enhanced concentrations of dissolved gaseous mercury in the surface waters of the Arctic Ocean. *Mar. Chem.* **2008**, *110* (3−4), 190−194.
(40) Poissant, L.; Amyot, M.; Pilote, M.; Lean, D. Mercury water-air exchange over the upper St. Lawrence River and Lake Ontario. *Environ. Sci. Technol.* **2000**, *34*, 3069−3078.
(41) Wilke, C. R.; Chang, P. Correlation of diffusion coefficients in dilute solutions. *AIChE J.* **1955**, *1* (2), 264−270.
(42) Wang, J.; Xie, Z.; Wang, F.; Kang, H. Gaseous elemental mercury in the marine boundary layer and air-sea flux in the Southern Ocean in austral summer. *Sci. Total Environ.* **2017**, *603−604*, 510−518.
(43) Wang, J. *Study on atmospheric Hg's transport in the boundary layer over the Antarctic inland and seas and its air-sea flux;* University of Science and Technology of China: Hefei, Anhui, China, 2018.
(44) Lamborg, C.; Rolfhus, K. R.; Fitzgerald, W. F.; Kim, G. The atmospheric cycling and air−sea exchange of mercury species in the South and equatorial Atlantic. *Deep Sea Res., Part II* **1999**, *46*, 957−977.
(45) Mason, R.; Fitzgerald, W. F.; Vandal, G. M. The sources and composition of mercury in Pacific Ocean rain. *J. Atmos. Chem.* **1992**, *14*, 489−500.
(46) Laurier, F. J. G.; Mason, R. P.; Whalin, L.; Kato, S. Reactive gaseous mercury formation in the North Pacific Ocean's marine boundary layer: A potential role of halogen chemistry. *J. Geophys. Res.-Atmos.* **2003**, *108* (D17), 1 DOI: 10.1029/2003JD003625.
(47) Whalin, L.; Kim, E.-H.; Mason, R. Factors influencing the oxidation, reduction, methylation and demethylation of mercury species in coastal waters. *Mar. Chem.* **2007**, *107* (3), 278−294.
(48) Strode, S. A.; Jaeglé, L.; Jaffe, D. A.; Swartzendruber, P. C.; Selin, N. E.; Holmes, C.; Yantosca, R. M. Trans-Pacific transport of mercury. *J. Geophys. Res.* **2008**, *113* (D15), 1 DOI: 10.1029/2007JD009428.
(49) Liss, P.; Merlivat, L. Air-sea exchange rates: introduction and synthesis. In *The role of air-sea exchange in geochemical cycling;* Buat-Menard, P., Ed.; D Reidel Publishing Company: Dodrecht, The Netherlands, 1986; pp 113−127.
(50) Wanninkhof, R. Relationship between wind speed and gas exchange over the ocean. *J. Geophys. Res.* **1992**, *97* (C5), 7373−7382.
(51) Wanninkhof, R.; McGillis, W. R. A cubic relationship between air−sea CO_2 exchange and wind speed. *Geophys. Res. Lett.* **1999**, *26* (13), 1889−18892.
(52) McGillis, W. R.; Edson, J. B.; Hare, J. E.; Fairall, C. W. Direct covariance air−sea CO_2 fluxes. *J. Geophys. Res.* **2001**, *106* (C8), 16729−16745.
(53) Andersson, M. E.; Gardfeldt, K.; Wangberg, I.; Sprovieri, F.; Pirrone, N.; Lindqvist, O. Seasonal and daily variation of mercury evasion at coastal and off shore sites from the Mediterranean Sea. *Mar. Chem.* **2007**, *104* (2007), 214−226.
(54) Lyman, S. N.; Jaffe, D. A. Formation and fate of oxidized mercury in the upper troposphere and lower stratosphere. *Nat. Geosci.* **2012**, *5* (2), 114−117.
(55) Parrella, J. P.; Jacob, D. J.; Liang, Q.; Zhang, Y.; Mickley, L. J.; Miller, B.; Evans, M. J.; Yang, X.; Pyle, J. A.; Theys, N.; Van Roozendael, M. Tropospheric bromine chemistry: implications for present and pre-industrial ozone and mercury. *Atmos. Chem. Phys.* **2012**, *12* (15), 6723−6740.
(56) Dibble, T.; Jiao, Y.; Lam, K.; Schwid, A.; Wilhelmsen, C. In *What modelers may need to add to mechanisms of global oxidation of gaseous elemental mercury initiated by bromine,* Proceedings of the 13th International Conference on Mercury as a Global Pollutant, Providence, Rhode Island, July 16−21, 2017; ICMGP, 2017.

DOI: 10.1021/acs.est.8b06205
Environ. Sci. Technol. 2019, 53, 5052−5061